



Quantification of Classified Nickel Species in Spent FCC Catalysts

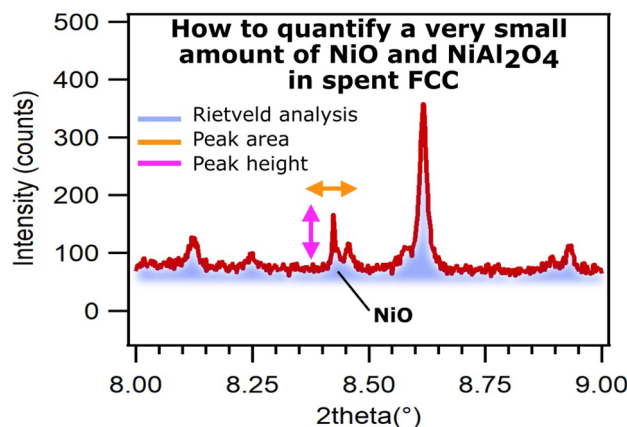
Monica Dapiaggi¹ · Marco Alloni² · Riccardo Carli² · Nicola Rotiroti¹ · Giorgia Confalonieri³

Received: 5 November 2020 / Accepted: 30 April 2021 / Published online: 12 May 2021
© The Author(s) 2021

Abstract

The paper presents a quick method for the quantification of nickel species in spent FCC catalysts; the quantification of known quantities NiO and NiAl₂O₄ is first done in a matrix of fresh zeolite Y, and then in a complex matrix, similar to the one of a real spent catalyst. The method is carefully checked and the errors in the quantification are critically evaluated. After the validation of the method with known quantities of NiO, well below the law limit for direct re-use, a set of real spent catalysts (representative of a period of 12 months) is analysed.

Graphic Abstract



Keywords NiO concentration · Quantification classified species · Spent catalysts

Statement of Novelty

The paper refers to the quantification of very small quantities of nickel compounds in complex matrices, with a detailed analysis of the possible issues connected. NiO identification and quantification is mandatory for waste recycling in a circular economy approach.

✉ Monica Dapiaggi
monica.dapiaggi@unimi.it

¹ Dipartimento di Scienze della Terra, Università degli Studi di Milano (I), Milano, Italy

² Prosimet S.p.A. (I), Filago, Italy

³ European Synchrotron Radiation Facility, Grenoble, France

Introduction

Fluid catalytic cracking (FCC) is an industrial process of extreme economical and environmental importance. It is an essential process for gasoline production and for the manufacturing of base chemicals. One of the most widely used active components for this process is a stabilized form of zeolite Y (faujasite), inserted in a composite particle, which also usually contains clays, alumina, and silica (as described in [1]).

The structure of zeolite Y comprises pores where large molecules can penetrate; moreover, thanks to the presence of acid sites, the pores can be converted to proper dimensions for the applications. Various alumina and silica sources are

added, in order to produce a meso- and macro-porous matrix; these materials, together with clays, also act as fillers [1].

Figure 1 shows a sketch of how most of the FCC processes work. Being the process endothermic, there's the need to start increasing the temperature, by burning some of the feedstock in the regenerator [1]. Hot catalyst material is combined with pre-heated feedstock at the bottom of the riser reactor ($T \approx 550^\circ\text{C}$). The reaction produces gases, that transport the catalyst/feedstock mixture up the riser reactor, at the top of which the temperature is a bit lower ($T \approx 500^\circ\text{C}$). The catalyst (still containing some carbon material) is separated from the product mixture and is transported to the regenerator, where it is burned off. The catalyst is thus regenerated and re-used continuously [2].

During the reaction-regeneration cycles, various modifications of the catalyst take place; moreover, heavy metals may accumulate in the catalyst (usually Ni, V, and Fe, which are contained in the crude oil in substantial amounts), poisoning it and thus reducing its catalytic performances. Meirer et al. [3] showed, in a particularly interesting paper and by means of element-specific nanotomography, where nickel and iron can be found in a spent FCC catalyst single particle, and how they likely poison the catalyst. They found out that Fe and Ni mainly accumulate at and near the surface of the particle, meaning that they entered the particle from the surface, i.e. during the catalytic process. Ni penetrates deeper than Fe into the particle with a peak concentration at about 300 nm and significant concentration levels up to 3 μm . What is really interesting, from the process point of view, is the correlation between porosity changes, relative elemental concentrations, and distance from the particle surface: from these comparisons, the authors could say that both Fe and Ni contaminate the particle from the outside, and that they tend to clog the macropore space, directly poisoning the catalyst, as also stated by Etim et al. [4] and Bai et al. [5].

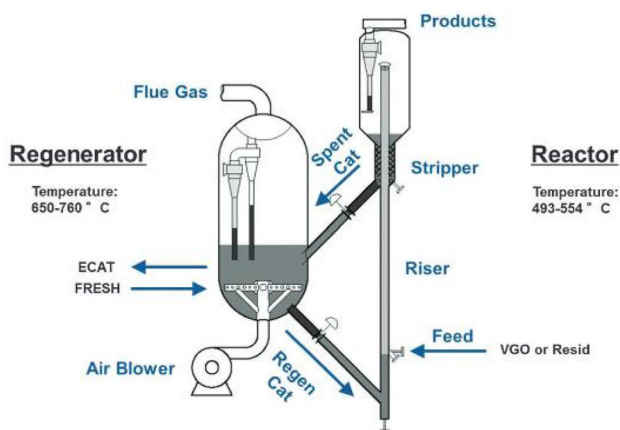


Fig. 1 Sketch of the fluid catalytic cracking process (FCC). Picture taken from [1]

Nickel is also problematic from the environmental point of view, especially for what concerns the disposal of the spent catalyst (or its direct re-utilization). In fact, some of the nickel compounds are classified as carcinogenic or toxic to reproduction (class 1A or 1B), so the presence of nickel must be carefully evaluated and quantified. Moreover, it is unavoidable to determine which crystalline species host the nickel content of the spent catalyst. Without this piece of information, a precautionary approach must be applied, considering thus the whole nickel content as belonging to the most dangerous species (i.e. NiO, bunsenite), which has a maximum law limit of 0.1 wt% [6]. If nickel content is over that limit, the spent catalyst must be classified as hazardous waste, and cannot be reused without a proper pre-treatment, that removes nickel compounds (or at least, reduces the concentration of nickel below the legal threshold). Busca and co-authors [7] showed that, in their samples, nickel oxide can be detected in small amounts, just larger than the legal limit, using X-ray powder diffraction. In the spent catalysts analysed, nickel was incorporated in the structure of Al_2O_3 , which has a spinel structure: the presence of Ni in the structure could be detected by the change in the cell parameter of the alumina itself. In a recent paper, Spadaro et al. [8] determined the detection limit of nickel and vanadium compounds, both from X-ray fluorescence (XRF) data and from X-ray diffraction (XRD) data, in a statistically meaningful way. They showed, in accordance to [7], that nickel can be present either in the structure of alumina, forming a defective Ni-Al spinel or in the amorphous phase that dominates the spent catalysts.

In the present paper, the authors would like to show how two nickel species (NiO and NiAl_2O_4) can be detected and quantified, even in the tiny quantities that represent the legal limit for waste classification [6], in a simplified matrix, as well as in a complex matrix such as the one of an FCC spent catalyst (for NiO). To do so, a three-step method was applied on high resolution X-ray diffraction data from synchrotron radiation: (i) quantification of added NiO in a fresh zeolite Y, down to 1000 mg kg^{-1} by means of Rietveld refinement, (ii) construction of calibration lines using peak area and peak intensity + testing in the quantification of known quantities of NiO and NiAl_2O_4 in a fresh zeolite Y, (iii) test of the calibration line with the quantification of known quantities of NiO added in a real spent catalyst matrix. The obtained outcomes provide a reliable quantification method of NiO, presents in a very low amount in a complex matrix. Nevertheless, our results allow us also to verify the accuracy of the evaluation, providing thus a consistent analysis protocol, complete with error evaluation in the quantification procedure. The whole procedure is then tested on a number of real FCC spent catalysts, coming from about 12 months sampling.

Experimental

Sample Preparation

Three sets of samples were prepared: (1) Na-zeolite Y (Alfa Aesar, CAS nr. 1318-02-1) with added NiO (Alfa Aesar, 99%, CAS nr. 12359) in decreasing amounts (from 20 wt% down to 0.1 wt%); (2) Na-zeolite Y with added NiAl₂O₄ spinel, in decreasing amounts (from about 0.25 wt% down to about 0.07 wt%); (3) a spent catalyst with added NiO, in decreasing amounts (from 1 wt% down to 0.05 wt%). The composition of all samples can be found in Table 1.

The NiAl₂O₄ spinel has been synthesised starting from stoichiometric quantities of nickel nitrate (Ni(NO₃)₂·6H₂O, Sigma Aldrich 99%, CAS nr. 13478-00-7) and aluminum nitrate (Al(NO₃)₃·9H₂O, Fluka, 98%, CAS nr. 13473-90-0), mixed carefully and heated up to 850 °C, in order to decompose the nitrates. The resulting powder was ground and calcined at 1100 °C for 5 h. The results of the synthesis were checked by means of X-ray powder diffraction, with a PANalytical X'Pert pro, equipped with a multichannel detector (X'Celerator), with Cu K α wavelength, a step size of about 0.02 °2 θ , and a counting time of 30 s step⁻¹.

All samples were carefully mixed in a ball mill for 5 min.

Data Collection and Rietveld Refinement

Data were collected at the ESRF, at the high resolution powder diffraction beamline ID22, with a wavelength of 0.354359 Å. The beamline detailed description can be found on the ESRF website [9]. The wavelength was set by a channel-cut Si(111) crystal monochromator. Diffracted intensity was detected, as a function of 2 θ , by a bank of nine scintillation detectors, each preceded by an Si(111) crystal analyzer. Measurements were performed in transmission, using a boro-silicate glass capillary with an internal diameter of 0.7 mm.

The Rietveld refinements were performed using GSAS-II [10]. The instrumental contribution to broadening was evaluated using LaB₆ (NIST SRM 660c), binned with a very small step size.

X-ray Fluorescence Analyses

X-ray fluorescence analyses were performed with a TIGER S8 spectrometer (Bruker) on glass pellets obtained with a Breitlander autofluxer. The recipe for the glass pellets was as follows: 1 g of sample powder and 8 g of a fluxer made by XRF services srl. The fluxer is composed of 66 wt% of lithium tetraborate, 34wt% of lithium metaborate, plus an added 0.2 wt% of lithium bromide. The glass pellets were then analyzed in the spectrometer, using a calibration line (for each element) obtained with standards mixed in various proportions. The software used is SPECTRA plus, version 3.0.2.8. The method is checked and validated everyday with mixtures with a known composition of the elements to be analyzed. Nickel, being in very small amounts, needed some extra work: the mixtures used for the calibration were made using very small amounts of nickel, for a better precision. Total carbon and sulphur were measured with an elemental analyser (Icarus G4, Bruker).

Results

Powder Diffraction Methods for the Quantification of NiO and NiAl₂O₄ in a Fresh Zeolite Y

In this section, three different methods (i.e. Rietveld refinement, calibration with peak area, and calibration with peak height) are tested for the quantification of NiO and NiAl₂O₄ added in known amounts to a fresh zeolite Y. The powder diffraction patterns of the samples with NiO (top graph) and of NiAl₂O₄ (bottom graph) can be found in Fig. 2. The peaks for bunsenite are clearly marked and still visible even at the lowest concentration. The red pattern in the top graph of Fig. 2 is the one without NiO, for a better visual estimation of the presence of bunsenite peaks. In the bottom graph of Fig. 2, the presence of nickel aluminum spinel is clearly visible down to the sample with 0.1wt%, while the situation is not so clear for the 0.047 wt% one (even though the most intense peak at 8.39°2 θ is still visible).

Rietveld Refinements

Rietveld refinements of all the samples containing zeolite Y and NiO were performed using an accurately refined structure for zeolite Y (on single phase diffraction data,

Table 1 Phase composition for all samples

Base	dopant	wt%	wt%	wt%	wt%	wt%	wt%
Zeolite Y	NiO	20	2	1	0.5	0.25	0.1
Zeolite Y	NiAl ₂ O ₄	0.25	0.12	0.047			
Spent catalyst	NiO	1	0.5	0.25	0.12	0.05	

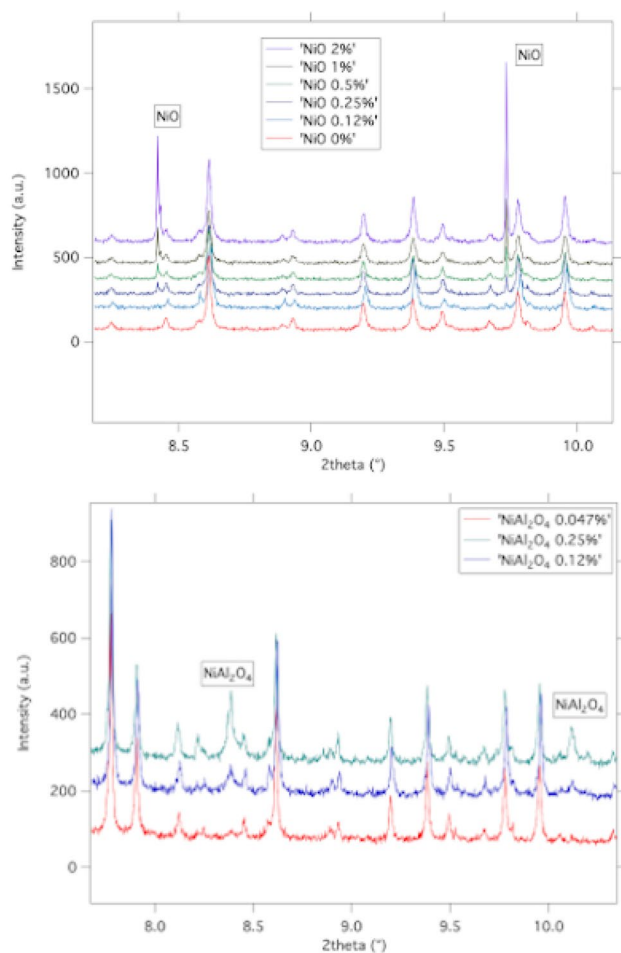


Fig. 2 Comparison of powder diffraction patterns of zeolite Y with known quantities of NiO (top graph) and with known quantities of NiAl_2O_4 (bottom graph). The sample with 20 wt% of NiO was omitted from the figure for a better clarity. The red curve in the top graph corresponds to pure zeolite Y, to better appreciate the presence of NiO

specifically collected). Structure reported in Polisi et al. [11], was used as initial model. Si–O distances were soft-constrained, gradually decreasing the weight of

the constrain (up to 10) after the initial stages. Extra-framework species were located into the zeolite porosities inspecting carefully the Fourier difference map of the electronic density and using the starting model, their location and species were determined considering the bond distances and the mutual exclusion rules. Species and their locations were similar to those reported in Polisi et al. [11], except for W1 water molecule that in our refinement presents an occupancy factor equal to zero. The results of the Rietveld refinements of the samples containing zeolite Y and bunsenite can be seen in Table 2, which shows the main parameters that were refined, with the standard errors (provided by the minimization procedure) on the last decimal place in brackets. The magnitude of the standard error on NiO refined parameters obviously increases with the decrease of the amount of NiO in the sample: for instance, the standard error on the cell parameters is on the fifth decimal place for the samples with the highest NiO concentration and goes up to the third decimal place for the less concentrated samples. The size and strain parameters of NiO were refined only for the sample with the largest concentration, and then used and kept fixed for all the others, because refining the microstructural parameters (i.e. when the peak intensity is very small) provides unreliable results and affects the accuracy of the phase quantification. Microstrain is a particularly sensitive parameter: its effect on the broadening of the peaks' tails produces integrated intensities that may be highly unreliable, with the consequent excess on the phase scale. An example of the actual fit, for an amount of NiO corresponding to 0.5 wt%, is shown in Fig. 3: it can be clearly appreciated that the small amount of NiO can still be easily (and reliably) fitted.

Table 3 provides the results of NiO quantification. The last two columns represent the difference between the nominal and the refined concentrations, and the relative difference % (i.e. $100 \cdot (\text{refined} - \text{nominal}) / \text{nominal}$). Similarly to what has been done for zeolite Y and NiO, known (and small) quantities of nickel aluminum spinel (NiAl_2O_4) have been quantified through Rietveld

Table 2 Results of the Rietveld refinements performed on the samples with zeolite Y and known quantities of nickel oxide

NiO (wt%)	NiO				zeolite Y			
	a (Å)	c (Å)	Size (μm)	Microstrain	a (Å)	Size (μm)	Microstrain	Rwp
20	2.95588 (3)	7.22979 (6)	6.8 (8)	656 (80)	24.5013 (3)	0.358 (4)	944 (44)	17.10
2	2.95582 (7)	7.2298 (2)	–	–	24.5147 (2)	0.387 (4)	1668 (36)	14.12
1	2.9559 (1)	7.2296 (3)	–	–	24.5160 (2)	0.398 (4)	1924 (35)	12.73
0.5	2.9557 (2)	7.2301 (5)	–	–	24.5170 (2)	0.394 (4)	1894 (36)	12.35
0.25	2.9559 (4)	7.229 (1)	–	–	24.5162 (2)	0.357 (4)	1623 (36)	14.06
0.1	2.956 (2)	7.230 (5)	–	–	24.4969 (4)	0.314 (4)	152 (64)	25.35

The first column represents the nominal concentration of nickel oxide (in wt%). The number in brackets represents the standard error on the last decimal place, taken from the Rietveld least-squares procedure

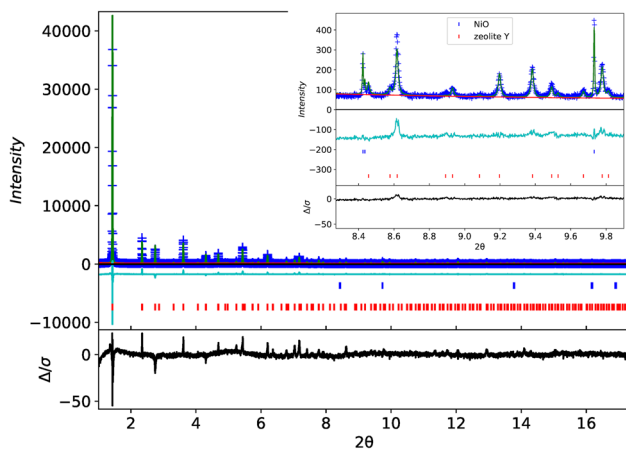


Fig. 3 Rietveld refinement results for zeolite Y spiked with 0.5 wt% of NiO. The black curve at the bottom represents the weighted difference between the observed and calculated diffraction pattern ($[\text{obs-cal}]/\sigma$); the square of this is what is actually minimized. In the inset, a zoom with two of the NiO peaks clearly visible

Table 3 Results of the phase quantification for NiO and NiAl_2O_4 with the Rietveld method

Dopant	Nominal wt%	Refined wt%	Difference	Rel. difference %
NiO	20.00	19.3 (1)	-0.7	-3.5
NiO	2.00	1.86 (4)	-0.14	-7.0
NiO	1.00	0.91 (3)	-0.09	-9.0
NiO	0.50	0.52 (3)	0.02	4.0
NiO	0.25	0.22 (2)	-0.03	-12.0
NiO	0.12	0.07 (8)	-0.05	-41.7
NiAl_2O_4	0.25	0.23 (2)	-0.02	-8
NiAl_2O_4	0.12	0.11 (8)	-0.01	-8.3
NiAl_2O_4	0.047	0.04 (3)	-0.007	-14.9

The number in brackets represents the standard error on the last decimal place, taken from the Rietveld least-squares procedure

refinement. The results of the quantification are shown in Table 3. The relative errors % were calculated in the same way as for NiO.

Calibration Lines Using Peak Areas and Peak Heights

An alternative method has been tested, in order to obtain a quick quantification of NiO and NiAl_2O_4 , and to study its accuracy in standard and in real samples. For this purpose, a calibration using the peak areas of NiO could be fast and reliable enough. Peak areas have been evaluated using a pseudo-Voigt function. The area of the main peak on NiO in zeolite Y (same samples as in Sect. 4.1.1) was calibrated against concentration, giving a regression line

with a $R^2 = 0.99975$ and a slope of 2.054, providing the concentration on NiO as $\frac{\text{peak-area}}{2.054}$. However, the area in peaks with such a small intensity is quite difficult to evaluate in a reliable way: the limits of the peaks are ill-defined, and it is always an issue to reliably evaluate how wide are the peaks vs background. Small errors in the fit can result in large errors on the area itself. Even though the peak area is generally considered far more reliable than the peak height, when used for quantification purposes, the situation is different when the peak intensity is very small. The peak height may be, in such ill-conditioned cases, a safer choice. Peak heights have been evaluated using a pseudo-Voigt function. Using peak heights, the regression line has $R^2 = 0.99983$ and a slope of 267.43, providing the concentration on NiO as $\frac{\text{peak-height}}{267.43}$. The same type of calibration has been done with NiAl_2O_4 , using both peak areas and peak heights, providing an $R^2 = 0.9702$ and a slope of 14.76 for the areas, and a $R^2 = 0.989$ and a slope of 308.35 for the heights.

The first check to be done is to understand how accurate we can be with these regression lines: in order to quantify the error made just because of the limited number of decimals in the calibration, we decided to use the regression lines to quantify the standard samples, i.e. the samples with known analyte amounts that were used to construct the calibration lines themselves. For this purpose, we quantified NiO and NiAl_2O_4 , with the area and the height calibration lines, in the same samples already described. Table 4 provides the details of this quantification.

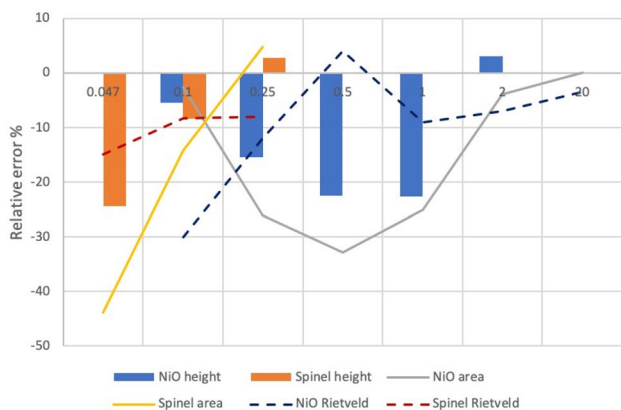
Comparison of the Various Methods

It is now interesting to compare the two methods and two dopants, in terms of their accuracy (defined here by the relative error %). Figure 4 shows such a comparison. The blue histogram and the grey line refer to NiO, with the height and the area regression method, respectively. The orange histogram and the yellow line refer to NiAl_2O_4 , with the height and the area regression method, respectively. We can observe, from the figure, that the relative errors % are systematically larger, in absolute value, for the area regression method than for the height one, for both NiO and NiAl_2O_4 . Moreover, it seems more difficult to get accurate values for spinel data than for NiO data, as the relative error % are systematically much larger for the NiAl_2O_4 , in accordance with the worse R^2 for the spinel regression lines.

Figure 4 also shows, with a dashed cyan line and with a red dashed line, the relative error % for the Rietveld quantification of NiO and of NiAl_2O_4 , respectively, in the same samples used for the regression line method. The comparison is not fair, because of the very different issues in the quantification for the two methods, but it is still edifying to make. The data, relative to the Rietveld results, are taken from Table 3. Apparently, the Rietveld method works best

Table 4 Results of the phase quantification for NiO and NiAl₂O₄ with the area and the height regression method in samples with fresh zeolite Y

Dopant	Method	Nominal	Calculated	Difference	Relative difference %
		wt%	wt%		
NiO	Area	20.00	20.029	0.029	0.15
NiO	Area	2.00	1.923	-0.077	-3.85
NiO	Area	1.00	0.750	-0.25	-25.02
NiO	Area	0.50	0.336	-0.164	-32.81
NiO	Area	0.25	0.185	-0.065	-26.00
NiO	Area	0.12	0.097	-0.023	-19.17
NiO	Height	20.00	20.009	0.009	0.04
NiO	Height	2.00	2.061	0.061	3.06
NiO	Height	1.00	0.774	-0.226	-22.60
NiO	Height	0.50	0.388	-0.112	-22.41
NiO	Height	0.25	0.212	-0.038	-15.34
NiO	Height	0.12	0.095	-0.005	-20.83
NiAl ₂ O ₄	Area	0.25	0.262	0.012	4.83
NiAl ₂ O ₄	Area	0.12	0.103	-0.017	-14.22
NiAl ₂ O ₄	Area	0.047	0.026	-0.021	-43.81
NiAl ₂ O ₄	Height	0.25	0.257	0.007	2.79
NiAl ₂ O ₄	Height	0.12	0.110	-0.010	-8.38
NiAl ₂ O ₄	Height	0.047	0.036	-0.011	-24.31

**Fig. 4** Comparison of the accuracy for the quantification with the regression line method, with peak areas and peak heights. Rietveld results are shown for comparison. Data are taken from Table 3

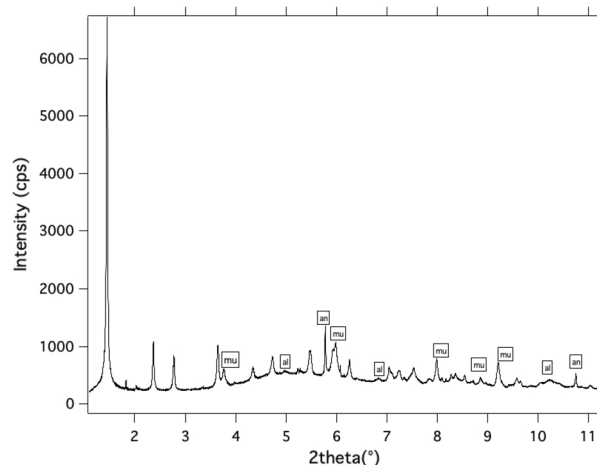
for the larger NiO concentrations, while it's not as accurate for the smaller ones. For what concerns NiAl₂O₄, with only three data points, it is difficult to comment sensibly.

Powder Diffraction Methods for the Quantification of NiO in a Real Spent Catalyst

Very small quantities of NiO and NiAl₂O₄ were detected with ease, when present in well crystallised fresh zeolite

Y, as shown in Sect. 4.1. However, the presence of these phases must be detected, in real life, in a complex matrix, such as the one of spent catalysts, containing various crystalline phases, and one or more amorphous ones, resulting in a structured and high intensity background. Figure 5 shows a multiphase diffraction pattern of a typical spent catalyst, where θ alumina was likely used as a support. The active catalytic phase (zeolite Y) is still present, even though with broader peaks; it clearly underwent some temperature driven decomposition reaction, as mullite is present in substantial amount. Anatase is usually present in FCC catalyst as an active matrix component and specifically as the active phase of vanadium traps [12, 13]. Moreover, the structured background is a sign that the process of thermal decomposition of zeolite Y was almost complete, as an amorphous phase is definitely present.

The phase identification has been performed by means of PANalytical Highscore plus [14]. With this sort of matrix, the identification and the quantification of nickel oxide and/or of nickel aluminum spinel can be challenging. In particular, the Rietveld method will not be easy to apply, as it requires an internal standard for the quantification of the amorphous component, with some issues on the accuracy [15]. The Rietveld method, in fact, normalises the phase fractions, so that their sum is 1. In this way, only crystalline phases are taken into account in the quantification, leading to a gross overestimation of the crystalline components (especially when the amorphous content is large, like in this case). The only way to use the Rietveld method, when an amorphous component is present, is to couple it with RIR method, by means of addition of an internal standard; the procedure, however, is long and complex, subjected to

**Fig. 5** Powder diffraction pattern of a typical spent catalyst sample with phase identification. Peaks labelled with 'mu' belong to mullite, those labelled with 'an' belong to anatase, and those labelled with 'al' belong to a θ alumina support. All the other peaks belong to zeolite Y

quite large errors in the amorphous content evaluation, and to issues in the choice of the proper internal standard [15].

The idea was then to check whether NiO was still detectable in a complex matrix: small amounts of NiO were added to a spent catalyst with a very low amount of nickel (determined by XRF, as shown in the experimental section). The usual 1 wt%, 0.5 wt%, 0.25 wt%, 0.1 wt%, and 0.05 wt% were added to the matrix. Figure 6 shows the corresponding powder diffraction patterns. The inset shows a zoom of the data, where NiO peaks are well visible above the background.

The samples of the spent catalyst with added NiO (Fig. 6) were used to check whether the calibration lines previously obtained were working also in complex samples with a high background. The presence of an amorphous phase, in fact, usually constitutes an issue in the quantification of very small amount of crystalline materials by means of powder diffraction. The introduction of known quantities of the studied species in one of such samples, should help to understand how and if the calibration lines are working in such ill-condition cases. In the same way as previously done, the calibration for peak area and peak heights were used and compared.

Table 5 shows the results. The peak areas and the peak height were determined using PANalytical Highscore plus [14].

The last column, i.e. the relative difference %, shows clearly that the height method performs much better than the area method with such small quantities. Even though the accuracy is not optimal, the method is very quick and reliable. The relative differences are much larger than those estimated for the samples with fresh zeolite Y (see for comparison Table 4). It is then clear that the complex nature of

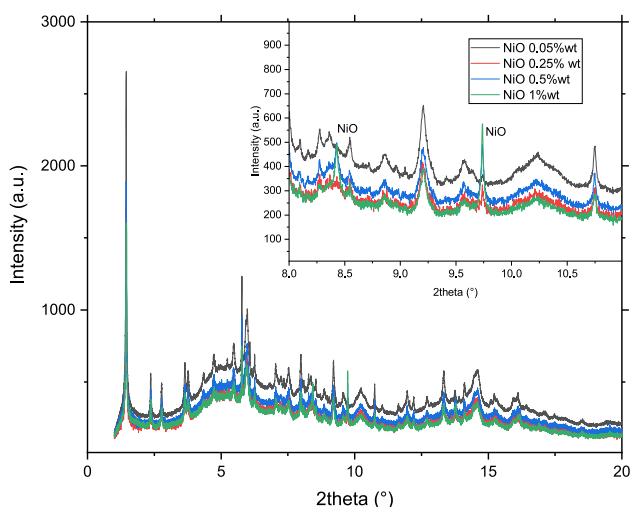


Fig. 6 Comparison of powder diffraction patterns of a spent catalyst with known quantities of NiO. In the inset, a zoom of the graph, where the peaks from NiO are clearly visible

Table 5 Results of the phase quantification for NiO in the spent catalyst using the peak areas and the peak heights

Dopant	Method	Nominal	Refined	Difference	Relative difference
		wt%	wt%		
NiO	Area	1	2.434	1.43	143
NiO	Area	0.5	2.244	1.74	349
NiO	Area	0.25	1.042	0.79	317
NiO	Area	0.12	1.232	1.11	927
NiO	Area	0.05	0.915	0.87	1730
NiO	Height	1	0.705	- 0.30	- 29
NiO	Height	0.5	0.417	- 0.08	- 17
NiO	Height	0.25	0.177	- 0.07	- 29
NiO	Height	0.12	0.1199	0.00	- 0.08
NiO	Height	0.05	0.079	0.029	58

the matrix, its many diffraction peaks and the presence of an amorphous component play a key role in determining the accuracy of the method. Regarding the results for NiO, it can be noted that the larger concentrations tend to be underestimated, but this is not true for the smallest one, which is largely overestimated. Even though the relative difference % of this particular sample is quite large, it goes in the right direction for a conservative approach to the environmental issue described in this paper. The results of this paragraph show that it is possible, quickly and easily, to evaluate a NiO concentration as low as 500 ppm; even taking into account the large positive uncertainty of the determination, the result will still be below the law limit of 1000 ppm.

Powder Diffraction Data and X-ray Fluorescence Analyses in a Set of Real Spent Catalysts

After the validation of the quantification method, the analysis of the issues connected to it, and the evaluation of the errors that can affect the measurement, the following step was to apply the method (and the corresponding minimum detectable quantity) to some real samples of spent catalysts. The samples are representative of quite a long period (12 months) and have been characterised first from the chemical point of view by means of XRF.

The results of the chemical analyses can be found in Table 6: nickel concentration, recalculated as 'NiO', varies between about 0.2 wt% and about 0.5 wt%.

X-ray powder patterns of all the samples were then checked for the presence (and eventual quantification) of nickel containing species. The graph in Fig. 7 shows the powder diffraction patterns collected for the real spent catalysts. The inset shows the region of interest for the species studied. It can be seen that no peak is present in the regions of the two main peaks for both species. Even

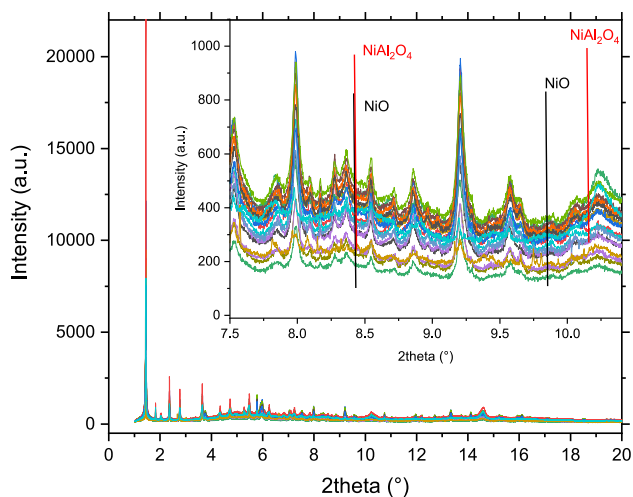


Fig. 7 Powder diffraction patterns for the spent catalysts. The inset represents the same data in the region of interest for NiO (black lines) and NiAl₂O₄ (red lines). (Color figure online)

though some doubt may arise for the region around $8.4^{\circ}2\theta$, the $9.7^{\circ}2\theta$ peak is not present; the latter is the most intense peak, while the one at $48.4^{\circ}2\theta$ has an intensity of 60% of the most intense. In the same way, NiAl₂O₄ is not present in the powder diffraction patterns. As we know that 0.05 wt% of NiO is still well detectable and quantifiable in a similar matrix, we can say that NiO is certainly below 0.05 wt%.

Conclusions

The paper shows a very quick and relatively accurate way to determine whether a spent catalyst sample contains NiO (with the corresponding concentrations, down to 0.05 wt%) and NiAl₂O₄, though only qualitatively.

A detailed study of known and very small concentrations of the two species in simple and more complex matrices provided the possibility to deeply understand their detection limit and the errors connected to their quantification. Various methods have been applied for the quantification, and the following conclusions can be drawn: - the Rietveld method is quite accurate and reproducible, but it can be applied only when the matrix is crystalline and not particularly complex; using it in complex matrices, with an amorphous component, requires an internal standard, and it is not particularly accurate, in general, for very low concentrations of the two studied species; - the peak area and peak height methods showed to be very fast and quite reliable in the samples with fresh zeolite Y: in particular, for the smaller concentrations, the peak height method provides better results; in a complex matrix, similar to the one of real spent catalysts, the presence of NiO is well visible (and quantifiable) down to a concentration of 0.05 wt%.

The concentration limit of NiO for the direct re-use of waste materials is 0.1 wt%: with the method proposed it is possible to determine whether the spent catalysts are directly recyclable. Even though the method needs to be carefully

Table 6 Sample composition for spent catalysts obtained with XRF-WDS analyses

Sample	LOI	C(tot) wt%	S(tot) wt%	SiO ₂ wt%	Fe ₂ O ₃ wt%	Al ₂ O ₃ wt%	CaO wt%	MgO wt%	Na ₂ O wt%	NiO wt%	TiO ₂ wt%	P ₂ O ₅ wt%
17-010	1.11	0.33	0.05	39.85	0.48	48.92	0.70	0.00	0.24	0.260	0.81	0.51
17-022	0.27	0.08	0.05	45.06	1.07	40.50	1.20	1.61	0.53	0.472	1.76	0.06
18-071	0.28	0.05	0.16	47.93	0.90	39.61	0.74	1.92	0.07	0.197	1.86	0.41
18-074	0.89	0.09	3.04	43.62	1.70	41.25	1.55	1.06	0.72	0.525	1.22	0.12
18-077	0.12	0.09	0.12	46.54	0.94	40.77	0.77	1.86	0.12	0.259	1.88	0.31
18-078	11.02	0.13	2.20	40.20	0.76	47.64	0.88	0.00	3.70	0.256	0.92	0.46
18-079	0.52	0.09	0.11	45.93	0.94	40.48	0.77	1.72	0.13	0.277	1.85	0.28
18-083	0.22	0.10	0.08	46.34	1.00	41.58	0.79	1.66	0.19	0.335	1.89	0.21
18-086	0.31	0.09	0.08	45.74	1.00	41.44	0.82	1.65	0.18	0.332	1.89	0.22
18-089	0.27	0.12	0.06	45.29	1.02	41.76	0.85	1.51	0.22	0.365	1.88	0.15
18-093	0.38	0.12	0.05	44.70	1.01	41.52	0.82	1.50	0.22	0.365	1.86	0.14
18-095	0.29	0.11	0.05	44.50	1.02	41.55	0.81	1.52	0.22	0.365	1.85	0.13
18-099	0.40	0.11	0.04	44.05	1.01	41.21	0.81	1.44	0.23	0.375	1.84	0.12
18-108	0.67	0.10	0.03	43.80	1.02	41.65	0.78	1.38	0.26	0.365	1.81	0.08
18-110	0.51	0.10	0.04	44.00	1.01	41.47	0.82	1.40	0.23	0.375	1.84	0.12
18-123	2.54	0.11	0.05	38.70	0.42	49.12	0.70	0.00	0.34	0.313	0.81	0.45
18-127	0.65	0.22	0.03	43.39	1.10	41.55	0.81	1.55	0.27	0.439	1.77	0.09
18-135	0.51	0.18	0.03	43.25	1.10	41.50	0.81	1.64	0.26	0.443	1.78	0.09
18-137	0.36	0.19	0.02	43.26	1.13	42.69	0.81	1.72	0.27	0.457	–	0.08

checked before applying it to different matrices/samples, the authors think that the way showed in this paper can be useful when extended to other situations. The use of a very high resolution powder diffraction beamline, such as ID22 @ESRF, provided very good results, because of its exceptional signal-to-noise ratio, and may be instrumental for the continuation of this work.

Acknowledgements The authors would like to thank the European Synchrotron Radiation Facility for providing beam time for experiments ES-609 and MA-3957, and Andy Fitch, Mauro Coduri, and Wilson Mogodi for their help during data collection.

Funding Open access funding provided by Università degli Studi di Milano within the CRUI-CARE Agreement. MD acknowledges the support of the Italian Ministry of Education (MIUR) through the Project -PRIN2017 - MINERAL REACTIVITY, A KEY TO UNDERSTAND LARGE-SCALE PROCESSES.

Declarations

Conflict of interest The authors declare that they have no conflict of interest.

Open Access This article is licensed under a Creative Commons Attribution 4.0 International License, which permits use, sharing, adaptation, distribution and reproduction in any medium or format, as long as you give appropriate credit to the original author(s) and the source, provide a link to the Creative Commons licence, and indicate if changes were made. The images or other third party material in this article are included in the article's Creative Commons licence, unless indicated otherwise in a credit line to the material. If material is not included in the article's Creative Commons licence and your intended use is not permitted by statutory regulation or exceeds the permitted use, you will need to obtain permission directly from the copyright holder. To view a copy of this licence, visit <http://creativecommons.org/licenses/by/4.0/>.

References

- Vogt, E., Weckhuysen, B.: Fluid catalytic cracking: recent developments on the grand old lady of zeolite catalysis. *Chem. Soc. Rev.* **44**, 7342–7370 (2015)
- Biswas, J., Maxwell, I.: Recent process- and catalyst-related developments in fluid catalytic cracking. *Appl. Catal.* **63**, 197–258 (1990)
- Meirer, F., Morris, D., Kalirai, S., Liu, Y., Andrews, J.: Mapping metals incorporation of a whole single catalyst particle using element specific X-ray nanotomography. *J. Am. Chem. Soc.* **137**, 102–105 (2015)
- Etim, U.J., Wu, P., Bai, P., Xing, W., Ullah, R., Subhan, F., Yan, Z.: Location and surface species of fluid catalytic cracking catalyst contaminants: implications for alleviating catalyst deactivation. *Energy Fuels* **30**, 10371–10382 (2016)
- Bai, P., Etim, U.J., Yan, Z., Mintova, S., Zhang, Z., Zhong, Z., Gao, X.: Fluid catalytic cracking technology: current status and recent discoveries on catalyst contamination. *Catal. Rev.* **61**, 333–405 (2019)
- Commission, E.: Classification, labelling and packaging regulation 790/2009/ce
- Busca, G., Riani, P., Garbarino, G., Ziemacki, G., Gambino, L., Montanari, E., Millini, R.: The state of nickel in spent fluid catalytic cracking catalysts. *Appl. Catal. A* **486**, 176–186 (2014)
- Spadaro, L., Arena, F., Di Chio, R., Palella, A.: Definitive assessment of the level of risk of exhausted catalysts: characterization of Ni and V contaminates at the limit of detection. *Top. Catal.* **62**, 266–272 (2019)
- Fitch, A.: <http://www.esrf.eu>
- Toby, B.H., Von Dreele, R.B.: GSAS-II: the genesis of a modern open-source all purpose crystallography software package. *J. Appl. Crystallogr.* **46**(2), 544–549 (2013)
- Polisi, M., Grand, J., Arletti, R., Barrier, N., Komaty, S., Zaarour, M., Mintova, S., Vezzalini, G.: CO₂ adsorption/desorption in FAU zeolite nanocrystals: in situ synchrotron X-ray powder diffraction and in situ Fourier Transform Infrared spectroscopic study. *Phys. Chem. C* **123**, 2361–2369 (2019)
- Hernandez-Beltran, F., Mogica-Martinez, E., Lopez-Salinas, E., Llanos-Serrano, M.E.: TPR and CO₂-TPD of composite titania (anatase)-alumina systems as potential vanadium traps for fluid catalytic cracking (FCC). *Stud. Surf. Sci. Catal.* **130**, 2459–2464 (2000)
- Martinez, N.P., Velasquez, J.R., Lujano, J.A.: Cracking heavy hydrocarbon feedstocks with a catalyst comprising anatase vanadium passivating agent. US Patent No. 4 816 135 (1989)
- Degen, T., Sadki, T., Bron, E., König, U., Nénert, G.: The High-Score suite. *Powder Differ.* **29**, S13–S18 (2014)
- Bernasconi, A., Dapiaggi, M., Gualtieri, A.F.: Accuracy in quantitative phase analysis of mixtures with large amorphous contents. The case of zircon-rich sanitary-ware glazes. *J. Appl. Crystallogr.* **47**, 136–145 (2014)

Publisher's Note Springer Nature remains neutral with regard to jurisdictional claims in published maps and institutional affiliations.